Acoustically levitated drops: drop oscillation and break-up driven by ultrasound modulation

A.L. Yarin [a,b,*], D.A. Weiss [c,d,e], G. Brenn [f], D. Rensink [f,1]

[a] *Faculty of Mechanical Engineering, Technion—Israel Institute of Technology, Haifa 32000, Israel*
[b] *Department of Chemical Engineering and Rheology Research Center, University of Wisconsin, Madison, WI 53706-1691, USA*
[c] *Laboratoire PMMH, ESPCI, 10 Rue Vauquelin, F-75231 Paris Cedex 05, France*
[d] *Department of Mechanical Engineering and Rheology Research Center, University of Wisconsin, Madison, WI 53706-1572, USA*
[e] *DaimlerChrysler Research and Technology, P.O. Box 23 60, D-89013 Ulm, Germany*
[f] *Lehrstuhl für Strömungsmechanik (LSTM), University of Erlangen–Nürnberg, Cauerstraße 4, D-91058 Erlangen, Germany*

Abstract

The behaviour of drops in an acoustic levitator is simulated numerically. The ultrasound field is directed along the axis of gravity, the motion of the drop is supposed to be axisymmetric. The flow inside the drop is assumed inviscid (since the time intervals considered are short) and incompressible.

First, as a test case, we consider a stationary ultrasound wave. We observe, as in previous experimental and theoretical works, that stable drop equilibrium shapes exist for acoustic Bond numbers up to a critical value. The critical value depends on the dimensionless wave number of the ultrasound. Beyond the critical value, we still observe equilibrium drop shapes, but they are not purely convex (i.e. "dog-bone" shaped) and found to be unstable.

Next we modulate the ultrasound pressure level (SPL) with a frequency ω_2, which is comparable to the first few drop resonance frequencies, and a small modulation amplitude. Simulations and experiments are performed and compared; the agreement is very good. We further on investigate numerically the more general case of an arbitrary ω_2 (still comparable to the first few drop resonance frequencies, yet). A very rich drop dynamics is obtained. We observe that a resonant drop break-up can be triggered by an appropriate choice of the modulation frequency. The drop then disintegrates although the acoustic Bond number remains below its critical value.

---

[*] Corresponding author. Tel.: +972-4-8293-473; fax.: +972-4-8324-533.
E-mail address: meralya@yarin.technion.ac.il (A.L. Yarin).
[1] Present address: Institut für Mikrotechnik Mainz, Carl-Zeiss-Str. 18-20, D-55129 Mainz.

Finally we change the modulation frequency linearly with time, sweeping over a window containing the drop's first eigenfrequency $\omega_2^{(\text{res})}$. After ω_2 has crossed $\omega_2^{(\text{res})}$, in the range of validity of the inviscid approximation, the drop equatorial radius oscillates between well-defined saturation values. For small modulations the range of oscillation grows linearly with the modulation amplitude. For larger modulations, however, a substantial increase in the oscillation range of the drop equatorial radius is observed in the case of down-sweep; the increase does not occur in up-sweeps of the modulation frequency. We compare our results with experimental findings and in particular the so-called jump phenomenon, as well as with experimental and numerical results from the literature. © 2002 Elsevier Science Ltd. All rights reserved.

1. Introduction

Acoustic levitators are a useful tool to suspend a drop without contact. This is interesting in connection with several industrial applications, e.g. containerless material processing, dryers or chemical reactors, etc. Ultrasound can also be used to atomize drops in a surrounding gas or to disperse them in a surrounding (immiscible) liquid.

The behaviour of drops in ultrasonic levitators is governed by the interaction between gravity and capillary forces, as well as the sound radiation pressure. From this it can already be seen what dimensionless groups are essential here, e.g. the gravitational Bond number, relating gravity to capillary effects, and the acoustic Bond number, relating acoustic to capillary effects.

To levitate a drop, the ultrasound has to be sufficiently strong to overcome gravity, otherwise the drop falls down. If the sound pressure level is too high, though, the drop disintegrates into small droplets, since then the capillary forces become too weak to keep the drop intact. Anilkumar et al. (1993) determined experimentally the critical acoustic Bond number, up to which stable static drop shapes occur, for several wave numbers of the ultrasound. The theoretical analysis by Lee et al. (1994) did not take gravity into account and underestimated the experimental values of the critical acoustic Bond number by about 13–20%.

For intermediate ultrasound pressure levels there are (stable) equilibrium drop shapes and positions, when the drops are steady and non-oscillating. These drop shapes deviate somewhat from a sphere, leading to a shift of the drop oscillation eigenfrequencies. For free drop oscillations, i.e. drops in the absence of gravity and acoustic field, Rayleigh found for low amplitude oscillations of spherical inviscid drops the eigenfrequencies of both axisymmetric and non-axisymmetric modes with $l \geqslant 2$ (see e.g. Lamb, 1932; Landau and Lifshitz, 1987)

$$\omega_l^{(\text{Ray})} = \left[\frac{l(l-1)(l+2)\sigma}{\rho R^3} \right]^{1/2}, \tag{1}$$

where l is the mode number, σ and ρ denote, respectively, the surface tension and the density of the fluid, and R the drop radius.

Eq. (1) is connected with a $(2l+1)$-fold degeneracy of the frequency spectrum, which means that for a given l the axisymmetric mode $m = 0$ has the same frequency $\omega_l^{(\text{Ray})}$ as all the corresponding $2l$ non-axisymmetric modes with $0 < |m| \leqslant l$ (Landau and Lifshitz, 1987). Eq. (1) yields

e.g. for water drops of $R = 1$ mm a frequency $f_l = \omega_l/(2\pi) \approx 121$ Hz for $l = 2$. This is much smaller than typical ultrasound frequencies $f_{US} = \omega_{US}/(2\pi)$, which in any case are beyond 20 kHz.

As reported by Shi and Apfel (1995) for an axisymmetric "pulsation" mode with $l = 2$ and $m = 0$, the shift of the eigenfrequency $\omega_2^{(res)}$ due to distortion of the drop equilibrium shape is positive (though small), i.e. towards larger eigenfrequencies, if the acoustic distortion of the drop from its spherical shape is small; the shift is negative, however, for larger distortions of the drop. Experimentally it was found in a low gravity environment (Trinh et al., 1996) that the eigenfrequency $\omega_2^{(res)}$ of the axisymmetric mode always decreases due to the drop squeezing by the acoustic field. The shift of the eigenfrequencies due to non-linear effects, i.e. to the coupling of different oscillation modes, was studied by Tsamopoulos and Brown (1983). They found a decrease of the eigenfrequencies $\omega_2^{(res)}$ with the square of the oscillation amplitude.

Droplet oscillations in a static sound field were recently studied by Murray and Heister (1999) under the assumption that the droplet radius was much smaller than the sound wavelength, and as a result, the gas motion was effectively incompressible. This restrictive assumption does not hold in many experiments with acoustic levitators, and a more general approach employing the Helmholtz equation instead of the Laplace equation is desirable to describe the gas motion.

Secondary streaming flows resulting from gas or droplet oscillations were recently studied by Lyell (1996), Yarin et al. (1999) and Yarin (2001). These effects involving viscous stresses are out of scope of the present work.

Note that Anilkumar et al. (1993) and Lee et al. (1994) reported on two equilibrium shapes for a given set of parameters in several cases of acoustic Bond numbers below the critical value. The two equilibrium shapes were distinguished by the equatorial radius of the drop; the drop with the smaller equatorial radius was purely convex, the one with the larger equatorial radius, however, had a "dog-bone"-like shape, its surface was thus partially concave. Both equilibrium shapes were apparently stable. However, using a projection of the phase space corresponding to the drop dynamics, Feng and Su (1997) argued that among the two drop shapes only one should be stable. The instability of the other corresponds to a saddle point in the projection of the phase space, in the neighbourhood of which the motion in the projection of the phase space is substantially slowed down. Some care is needed nevertheless in using this kind of argument, since their consideration only uses a projection of the phase space, not the whole phase space. A "separatrix" in the projection is therefore not necessarily separating different domains, but may be crossed (in the projection only!) by trajectories via the dimensions of the phase space which are excluded in the projection.

Modulation of the ultrasound offers additional possibilities to control the dynamics of free liquid surfaces and to intensify heat and mass transfer between levitated droplets and their environment. Marston and Apfel (1979, 1980), Trinh et al. (1982) and Trinh and Wang (1982) modulated the acoustic field in immiscible liquid–liquid systems, Marston and Goosby (1985) achieved drop breakup in modulated acoustic fields in liquid–liquid systems, Trinh et al. (1996) and Trinh et al. (1998) used it to excite particular modes of drop oscillations in the electrostatic levitator, whereas Marr-Lyon et al. (1997) used it to stabilize a liquid bridge.

Trinh and Wang (1982) and Daidzic et al. (1994) modulated the sound field linearly with time. The lowest eigenfrequency of the drop was within the interval swept. Trinh and Wang (1982) explored the resonance curves of the drop oscillation for different excitation amplitudes. Interestingly enough, they got an increase of the lowest drop eigenfrequency $\omega_2^{(res)}$ with an increase of

the oscillation amplitude, if the driving was provided by modulation of the single standing ul-trasound wave; the opposite was obtained when the driving was performed by modulation of a higher harmonic added to the basic ultrasound wave. Nothing is reported on a possible hysteresis, though. The experimental data obtained in Daidzic et al. (1994) are not easy to compare with theoretical results, since several parameters that are important from the physical point of view, e.g. sound pressure level, modulation amplitude, etc., are virtually not known. Furthermore, the amplitude of the sound generated depends linearly on the voltage at the generator only within a limited range. Therefore a linear modulation of the sound generator voltage does not necessarily lead to a linear modulation of the ultrasound pressure. This makes it difficult to interpret or even to reproduce the results of Daidzic et al. (1994).

The aim of the present work is to study the dynamics of droplet oscillations in the modulated acoustic field. The experimental equipment used to check the numerical results is presented in Section 2. The mathematical problem is posed in Section 3. Effects of the static acoustic field are numerically considered in Section 4 as test cases. Section 5 deals with the acoustic field effects in the case of a constant modulation frequency. In Section 6 the results are compared with exper-imental findings. Sweeping of the modulation frequency in time is treated in Section 7. The conclusions are presented in Section 8.

2. Experimental procedure

For the experiments, the ultrasonic levitator already used by Yarin et al. (1999) was employed together with an image analysis system for determining the droplet shape. The whole experimental apparatus is sketched in Fig. 1. The ultrasonic levitator supplied by Batelle Frankfurt (Germany) is characterized by the vibration frequency of the ultrasound transducer of 56 kHz. This frequency corresponds to the nominal sound wavelength $\lambda_0 = 6.1$ mm at an unperturbed air temperature $T_0 = 293$ K, where the unperturbed sound velocity in air is $c_0 = 343.8$ m/s. It was shown in Yarin et al. (1998) that the harmonic content of the acoustic field in the levitator may be approximated safely by a single standing harmonic wave. The ultrasound waves are reflected from the concave surface of a round reflector plate positioned opposite the transducer at a distance of 28.6 mm, which is appropriate to allow the formation of eight pressure nodes in this resonator. The distance
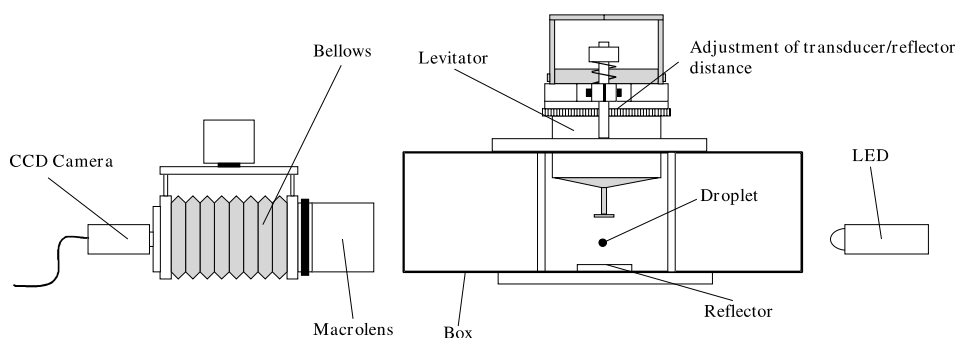

Fig. 1. Sketch of the experimental apparatus.

between the transducer and the reflector could be adjusted. The relative positions of the transducer and reflector were kept constant throughout the measurements, and no active control of the sound pressure level (SPL) was applied. Note that in the present case additional interactions between the droplet and the sound field, resulting from the finite dimensions of the chamber, which could destabilize positioning of the droplet (Rudnick and Barmatz, 1990; Feng and Su, 1997) were insignificant.

The droplets to be investigated were produced using a microlitre syringe. The desired drop volume was realized with an uncertainty of ± 0.05 μl. For producing the drop, the liquid was sucked into the syringe, and the volume of liquid representing the initial drop volume was pressed out of the syringe needle after it has been put close to the ultrasonic resonator. The drop was then inserted into the ultrasonic field, where the SPL had to be raised to overcome the adhesion forces which attach the drop to the needle. After the subsequent adjustment of the appropriate steady SPL at which the experiment was to be conducted, the drop was ready for the measurements. The SPL was determined from the aspect ratio of the drop shape for a given liquid and drop volume (cf. Yarin et al., 1998).

Oscillations of the droplet shape were obtained by a sinusoidal modulation of the amplitude A_0 of the incident pressure field with angular frequency ω_2 as described by

$$A_0^{(\text{eff})} = A_0(1 + \varepsilon \sin \omega_2 t) \quad \text{with } 0 < \varepsilon \ll 1. \tag{2}$$

The modulation of the SPL was achieved by driving the ultrasound transducer of the levitator with an amplitude-modulated electrical signal. This signal was produced by a waveform generator Yokogawa AG 1200. The frequency of the amplitude modulation was approximately the same as the eigenfrequency for the desired mode calculated by Eq. (1).

For determining the droplet shapes an imaging system was used. The particular parts of the system were a CCD video camera with macrolens and a PC equipped with a frame-grabber card and the software OPTIMAS. For imaging, the drop was illuminated from behind using a light-emitting diode (LED). The LED was triggered by a TTL signal generated by the waveform generator synchronous to the signal which drove the transducer. The LED yielded high-intensity light flashes with the length of 10 μs. This was short enough to ensure sufficiently sharp images of the droplet even when the surface velocities were largest. The trigger signal was coupled with the amplitude modulation. Thus the droplet was illuminated always in the same state of deformation in the oscillating period. To obtain droplet shapes at different deformation states, the phase shift between the amplitude modulation and the LED trigger signal was varied.

As a working fluid *n*-hexadecane $C_{16}H_{34}$ has been used. Since the evaporation of *n*-hexadecane droplets is significant only at time scales of hours, there was no need to visualize all shapes for one sequence of images during one and the same oscillation period. The procedure to visualize all shapes representing one complete oscillation was as follows: After recording the shape at one instant, the phase shift between the amplitude modulation of the SPL and the trigger signal for the LED was altered to visualize and record a different state of deformation. The time between two shape acquisitions was about 15 s. A full sequence was made up of 15 measurements, so that the overall time for visualizing one sequence of images as shown in Fig. 2 was 225 s, although they actually cover the oscillation period $T = 12.5$ ms. Since this is a short time interval compared to the time scale of evaporation, there was no need to account for changes of the drop volume or aspect ratio by adapting the SPL modulation frequency or amplitude. In Yarin et al. (1999) it was
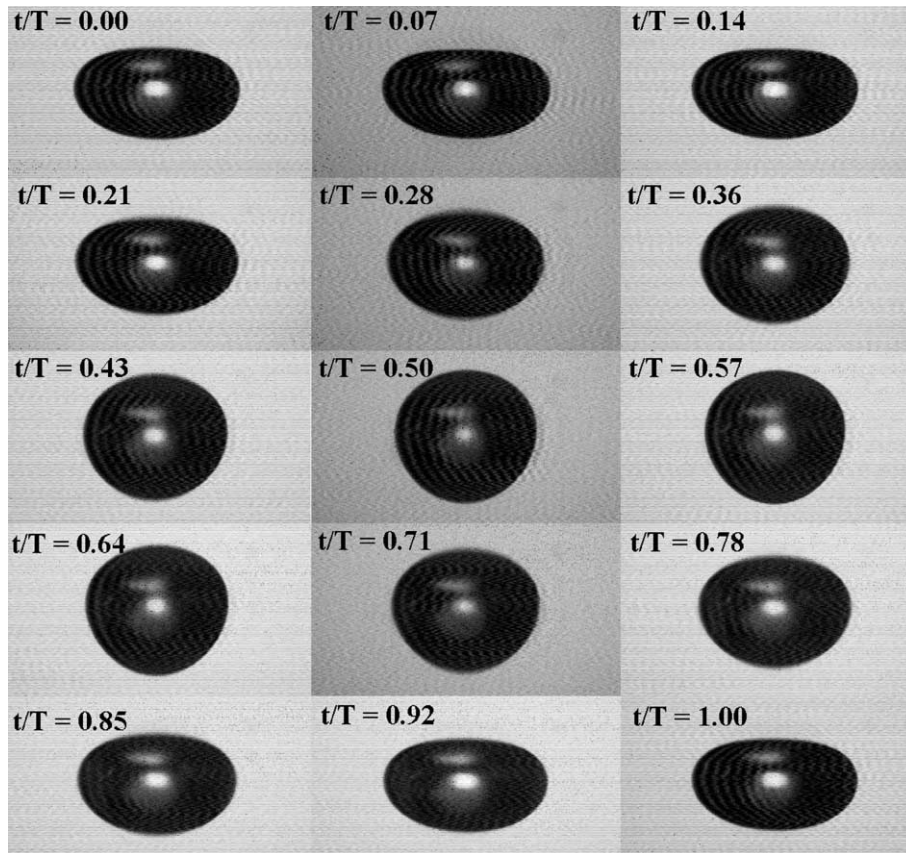
Fig. 2. Images of an *n*-hexadecane droplet in the mode $l = 2$ (dimensional volume 5.18 μl, $b/a = 1.4$) at different states of deformation. $T = 12.5$ ms represents the period of one full droplet oscillation. Maximum oblate deformation is at $t/T = 0.07$ and maximum prolate deformation is at $t/T = 0.57$.

shown that liquid vapour from the droplet is accumulated in the toroidal vortices induced by the ultrasonic standing wave above and below the droplet equator. To obtain a controlled droplet environment with respect to concentration of liquid vapour (and therefore the droplet temperature), these vortices had to be ventilated using a slight air flow directed towards the droplet. Since the present *n*-hexadecane droplet does not evaporate significantly, such measures for regulating vapour concentration were unnecessary. The air around the levitated droplet in the box shown in Fig. 1 was kept at the lowest possible relative humidity below 1%.

The drop was imaged using a large magnification factor, which was determined before the measurement series by imaging a high-precision microscale etched on a glass plate. The image analysis software provides detailed information on the visible meridional section of the drop. The data consist of the coordinates of points of the imaged droplet contour, the lengths of the major and minor semiaxes b and a and the aspect ratio b/a of the ellipse which approximates the drop shape. If the droplet image was ideally sharp, the accuracy of such an approximation was better than 2% in the representation of the major and minor semiaxes. Maximum sharpness was ob-

tained when the droplet was in the extreme states of deformation, where surface velocities vanish. In the intermediate stages between the two shapes of extreme deformation, the velocity of the droplet surface has a maximum. At these stages the droplet shape was slightly blurred, and therefore the accuracy in determining the minor and major axes as well as the captured droplet shape was slightly less than perfect. The accuracy here was of the order of 5%. Images of different states of deformation during the oscillation of an n-hexadecane droplet with a volume of 5.18 μl, which corresponds to $R = 1.07$ mm, and an unperturbed aspect ratio of 1.4 are depicted in Fig. 2. The various instants in the oscillation period to which the images correspond are represented by the non-dimensional time t/T, where T is the duration of the oscillation period of 12.5 ms in this experiment. The slightly varying sharpness of the droplet contour can be seen. The images are sharpest along the whole meridional circumference at $t/T = 0.07$ (maximum deformed oblate shape) and $t/T = 0.57$ (maximum deformed prolate shape), whereas all other images are slightly blurred due to the surface motion. Maximum blurred droplet contours can be seen at $t/T = 0.28$ and 0.78, when the droplet is in the mid-stage between the maximum oblate and prolate ellipsoidal shape and exhibits maximum surface velocities.

3. Formulation of the problem

We consider the behaviour of a drop under the influence of an external ultrasound field. Surface tension and gravity are taken into account, whereas liquid compressibility and viscous effects are neglected. The latter assumption imposes a restriction on the time interval when the inviscid approximation holds and viscous effects are still unable to damp out the oscillation mode corresponding to the lowest eigenfrequency. An estimation of the time interval will be given in Section 4.2.

The velocity field $\mathbf{u}$ is therefore irrotational and contains neither sources nor sinks; it can be described by a scalar potential Φ as per

$$\mathbf{u} = \operatorname{grad} \Phi \tag{3}$$

with

$$\Delta \Phi = 0. \tag{4}$$

The non-steady Bernoulli integral evaluated at the surface of the drop can be transcribed to

$$\frac{\mathrm{D}\Phi}{\mathrm{D}t} = \frac{1}{2}(\operatorname{grad}\Phi)^2 - gz - \frac{p}{\rho}, \tag{5}$$

where $\mathrm{D}/\mathrm{D}t = \partial/\partial t + \mathbf{u} \cdot \operatorname{grad}$ stands for the material time derivative, g denotes the acceleration due to gravity in $(-z)$-direction. The pressure p in the liquid is due to the capillary pressure and the radiation pressure of the ultrasound field:

$$p = p_{\mathrm{cap}} + p_{\mathrm{rad}} \tag{6}$$

with

$$p_{\mathrm{cap}} = \sigma\left(\frac{1}{R_1} + \frac{1}{R_2}\right), \tag{7}$$

where R_1 and R_2 are the curvature radii of the drop surface. The frequency of the ultrasound is much larger than the first eigenfrequencies of the drop. The latter thus "feels" only the temporal mean of the acoustic pressure field, i.e.

$$p_{rad} = \frac{1}{2}(\rho_0 c_0^2)^{-1}\langle p'^2 \rangle - \frac{1}{2}\rho_0\langle \mathbf{v}'^2 \rangle + \text{higher order terms,} \tag{8}$$

with ρ_0 being the density of the ambient gas. Also $\mathbf{v}'$ is the speed of the gas due to sound wave propagation, acute brackets denote time average and primes amplitudes of oscillation.

In (8) $\mathbf{v}'$ can be expressed by the pressure fluctuation in the gas p' via

$$\langle \mathbf{v}'^2 \rangle = \omega_{US}^{-2}\rho_0^{-2}\langle(\text{grad}\, p')^2\rangle, \tag{9}$$

where ω_{US} is the angular frequency by the ultrasound. The sound field is composed by an incident field p_{inc} and a scattered field p_{scat}

$$p' = p_{inc} + p_{scat}. \tag{10}$$

Both p_{inc} and p_{scat} (as well as their sum p') satisfy the Helmholtz equation

$$(\Delta + k^2)p' = 0 \tag{11}$$

with the wave number $k = \omega_{US}/c_0$, subject to the boundary conditions,

$$\frac{\partial p'}{\partial n} = 0 \text{ at the drop surface} \tag{12}$$

and

$$p' \rightarrow p_{inc} \text{ at infinity.} \tag{13}$$

We assume cylindrical symmetry of the whole process. We thus only have to care about the radial and axial coordinates x and z, respectively, where x is restricted to positive values. In our considerations the incident sound wave is a standing wave in z-direction with an antinode at $z = 0$. Thus, if gravity were negligibly small, stable equilibrium positions could be found at

$$z = \left(n + \frac{1}{2}\right)\frac{\pi}{k}, \tag{14}$$

n being any integer.

We relate lengths to the volume equivalent drop radius R, velocities to $(gR)^{1/2}$, time to $(R/g)^{1/2}$, and the velocity potential to $(gR^3)^{1/2}$. The Bernoulli integral (5) in the non-dimensional form reads (neglecting higher order terms in the radiation pressure)

$$\frac{D\Phi}{Dt} = \frac{1}{2}(\text{grad}\,\Phi)^2 - z - S\left(\frac{1}{R_1} + \frac{1}{R_2}\right) - \frac{1}{2}SB_a\{\langle p'^2 \rangle - \kappa^{-2}\langle(\text{grad}\,p')^2\rangle\}. \tag{15}$$

The following dimensionless groups are involved: the inverse gravitational Bond number

$$S = \frac{\sigma}{\rho g R^2}, \tag{16}$$

the acoustic Bond number

$$B_a = \frac{A_0^2 R}{\rho_0 c_0^2 \sigma} \tag{17}$$

(where A_0 denotes the amplitude of the incident pressure field p_{inc}), and the non-dimensional wave number of the ultrasound

$$\kappa = kR. \tag{18}$$

The assumption that $\kappa \ll 1$ is not made in the present work, and therefore the Helmholtz equation (11) is not replaced by the Laplace equation, as it has been done by Murray and Heister (1999).

Later on, we will neglect gravity, considering droplet oscillations and break-up. We then render time non-dimensional by $(\rho R^3/\sigma)^{1/2}$, velocities by $(\rho R/\sigma)^{-1/2}$, and the velocity potential by $(\sigma R/\rho)^{1/2}$. The Bernoulli integral then reads (higher order terms in the radiation pressure again neglected)

$$\frac{\mathrm{D}\Phi}{\mathrm{D}t} = \frac{1}{2}(\mathrm{grad}\,\Phi)^2 - \left(\frac{1}{R_1} + \frac{1}{R_2}\right) - \frac{1}{2}B_a\{\langle p'^2 \rangle - \kappa^{-2}\langle(\mathrm{grad}\,p')^2\rangle\}. \tag{19}$$

The evolution of the free surface shape is governed by the kinematic condition

$$\frac{\mathrm{D}\boldsymbol{x}}{\mathrm{D}t} = \mathrm{grad}\,\Phi. \tag{20}$$

We want to simulate numerically the evolution of the free surface itself (i.e. its x- and z-coordinates) as well as of the potential Φ at the free surface according to Eq. (20) and Eqs. (15) or (19), respectively. We make use of a boundary-element method to determine the normal derivative $\partial\Phi/\partial n$ at the surface of the drop from the integral equation

$$\Phi(\mathbf{x}) = \int \left\{ G(\mathbf{x}, \mathbf{x}')\frac{\partial\Phi}{\partial n'} - \Phi(\mathbf{x}')\frac{\partial G(\mathbf{x}, \mathbf{x}')}{\partial n'} \right\}\mathrm{d}A', \tag{21}$$

if $\mathbf{x}$ is on the surface of the drop. Φ is known on the drop surface. The integration expands over the surface of the drop. Also $\mathrm{d}A'$ denotes the surface element of the drop at $\mathbf{x}'$, n' the outer unit normal vector at $\mathbf{x}'$, and G Green's function for the Laplacian. Details on the numerical method including analytical integration in the azimuthal direction can be found elsewhere (Becker, 1992; Weiss and Yarin, 1999).

The distribution of the radiation pressure p_{rad} is determined via Eq. (8) with the higher order terms neglected and using Eqs. (9)–(11). The scattered pressure distribution p_{scat} is calculated from the known incident field p_{inc} by solving the integral equation

$$p_{scat}(\mathbf{x}) = \int \left\{ p_{scat}(\mathbf{x}')\frac{\partial H(\mathbf{x}, \mathbf{x}')}{\partial n'} + H(\mathbf{x}, \mathbf{x}')\frac{\partial p_{inc}}{\partial n'} \right\}\mathrm{d}A', \tag{22}$$

where use has been made of the boundary condition (12). As in (21), the integration expands over the surface of the drop. H denotes the (complex-valued) Green function for the operator $(\Delta + k^2)$. Details are given in Yarin et al. (1998).

The numerical solution of Eq. (21) has been tested against existing analytical solutions for small amplitude oscillations, as well as for non-linear droplet oscillations. In particular, it has
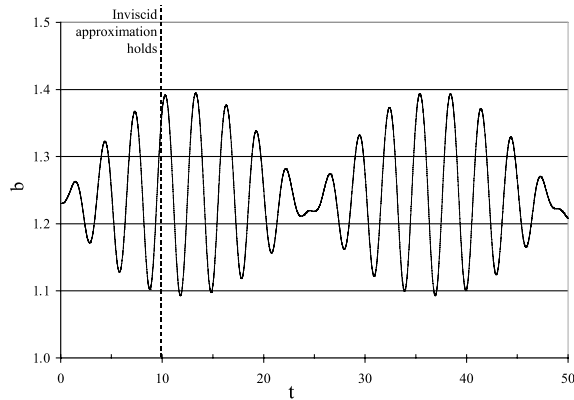
Fig. 3. The equatorial radius as a function of time for $\kappa = 0.575$, $B_a = 2.15$, $\varepsilon = 0.02$, and $\omega_2 = 2.0$.

reproduced very accurately the results for free non-linear oscillations shown in Fig. 3 of Lundgren and Mansour (1988), as well as some data of Shi and Apfel (1996) and Lee et al. (1994) briefly discussed in Section 4.1 and of Feng and Su (1997) in Section 4.2. The numerical solution of Eq. (22) has been tested in Section 3 of Yarin et al. (1998) against existing analytical results for acoustic scattering from a solid sphere and for levitation force acting on it, and showed high accuracy.

4. Static sound field: test cases

We consider here the behaviour of drops in an ultrasound field with a spectrum that contains only frequencies that are very large as compared to the first eigenfrequencies of the axisymmetric drop oscillations. This is what is meant here by a static sound field.

4.1. Equilibrium shapes

The predicted equilibrium drop shapes (oblate spheroid-like and "dog-bone"-like) were found to be in agreement with the theoretical results of Lee et al. (1994) and with the experimental data of Anilkumar et al. (1993). In particular, in the results of this section drop disintegration occurs via pinching-off of a torus-shaped volume at the equator, for example for $B_a = 2.25$ and 2.5. For acoustically small drops ($\kappa = 0.30$) and without gravity this was also observed numerically by Shi et al. (1995) and experimentally by Anilkumar et al. (1993). In the cases considered here, we did not observed any breaking membrane within a liquid torus, as shown in Section 5 below for modulated ultrasound. The torus-shaped volume at the equator has a cross-sectional radius $r_t \approx 0.001$ for $B_a = 2.25$ and 2.5 (r_t is rendered dimensionless by R). According to Rayleigh's theory of capillary instability, the torus should disintegrate into fragments corresponding to the fastest growing mode $\chi^* = 0.697$ (Chandrasekhar, 1961). Since the dimensionless wave number χ^* of the capillary instability is $\chi^* = 2\pi r_t / \Lambda^*$, where Λ^* is the wave length, the fragment length is

$\Lambda^* = 2\pi r_t/0.697$, and the volume, accordingly, is equal to $\pi r_t^2 (2\pi r_t/0.697) \approx 28.3 \times 10^{-9}$. The corresponding growth rate of the perturbations is $\gamma \approx 0.343 \, (Sr_t^{-3})^{1/2}$ (Chandrasekhar, 1961, we use $(R/g)^{1/2}$ as the time unit). With $S \approx 2$ therefore, the characteristic dimensionless time of the capillary instability of the shedded liquid torus is $\gamma^{-1} \approx 65 \times 10^{-6}$. This is virtually instantaneously, since the dimensionless time relevant for the drop dynamics is much larger ($t = O(1)$). Such a capillary break-up leading to the appearance of a number of fine secondary droplets in a ring-like region about the equator of the primary droplet actually means a loss of the axial symmetry of the flow.

4.2. Drop oscillations

We now consider the behaviour of drops that have shapes different from equilibrium ones at the beginning. In practice, this case is much more important, since the drops have to be put somehow into the ultrasound field, and in general they do not possess equilibrium shapes at that moment. So they start to oscillate.

The time unit is now $T_0 = (\rho R^3/\sigma)^{1/2}$, since we do not account for gravity. According to Lamb (1932) and Becker et al. (1991) viscosity μ damps the lowest eigenmode of the free oscillations of a droplet on the time scale $T_2 = \rho R^2/(5\mu)$. Denoting t^* and t dimensional and dimensionless time, respectively, we estimate for the time interval, where the inviscid approximation holds, as $t^* < T_2$. Therefore, it holds when

$$t < \frac{(\rho \sigma R)^{1/2}}{5\mu}. \tag{23}$$

Substituting the data for an n-hexadecane droplet of $R = 1.07$ mm, $\rho = 775$ kg/m³, $\sigma = 27.7$ mN/m and $\mu = 3.51$ mPa s (the physical quantities taken at 20 °C), we obtain from (23) that the inviscid approximation holds for about $t < 10$, which corresponds to $t^* < 50$ ms. Therefore, all inviscid results corresponding, say, to $0 \leqslant t < 10$ practically cannot be modified by viscous effects. During this time interval the oscillation mode corresponding to the lowest eigenfrequency is still unaffected by viscous effects, and practically there is no need to account for them. If we consider nevertheless drop oscillations beyond $t = 10$ in some cases later in this paper, this is to obtain information on a limiting behaviour; if a drop break-up or a blow-up of the oscillation amplitude does not occur even in the inviscid approximation, it will definitely not occur either if viscous effects are taken into account. Moreover, since the inviscid model keeps all the modes (with $l \geqslant 2$) undamped, the fact that a droplet does not disintegrate in theory definitely means that it does not disintegrate in reality either when damping is present. The same inviscid approximation was used to describe droplet oscillations in Tsamopoulos and Brown (1983) and Pelekasis et al. (1991).

In the simulations we put an ellipsoidal drop into the levitator. We mainly confirmed the results of Feng and Su (1997) on droplet oscillation and break-up in a static sound field. The results can be summarized by the statement that all equilibrium drop shapes found with an equatorial radius b below 1.8 are stable, and their small perturbation leads to oscillations, whereas all drop shapes with b beyond 1.8, in particular the dog-bone-like shapes, are unstable; their perturbation leads to break-up.

5. Monochromatically modulated ultrasound

We now modulate the amplitude A_0 of the ultrasound in time with an angular frequency ω_2 which is comparable to the first eigenfrequencies of the axisymmetric drop oscillations, according to

$$A_0^{(\text{eff})} = A_0(1 + \varepsilon \sin \omega_2 t) \quad \text{with } 0 < \varepsilon \ll 1. \tag{24}$$

We use $\kappa = 0.575$ throughout the section and neglect gravity here, therefore in the dimensionless variables sketched in Section 3 the angular frequency of the first resonance of a spherical drop in the linear regime becomes (Lamb (1932), cf. (1) with $l = 2$)

$$\omega_2^{(\text{Ray})} = 8^{1/2} \approx 2.828. \tag{25}$$

For the following calculations we take an acoustic Bond number (based on A_0) $B_a = 2.15$. Starting from this value, we determine equilibrium drop shapes for different stationary sound amplitudes $A_0(1 + \varepsilon)$ and find stable equilibrium drop shapes up to $\varepsilon = 0.08$, whereas we do not find any (for stationary ultrasound) for $\varepsilon \geqslant 0.09$. This corresponds to a critical acoustic Bond number $B_a^{(\text{crit})} = 2.15(1 + 0.09)^2 \approx 2.55$ and is in agreement, indeed, with the findings of Section 4.1, where the critical Bond number for $\kappa \approx 0.58$ was slightly above 2.50. The simulations using a modulated sound field always start from the equilibrium drop shape obtained for $\varepsilon = 0$.

In the absence of gravity the drop shape, due to obvious reasons, should be symmetric with respect to its equatorial plane throughout the oscillations, and the droplet centre should be located at the pressure node all the time. The code indeed reproduces this behaviour.

By weakly modulating the sound pressure amplitude with ω_2 close to the first eigenfrequency $\omega_2^{(\text{res})}$ of the drop, we typically obtain a beat between the eigenfrequency and ω_2. Fig. 3 shows the equatorial radius of the drop under a modulation with $\varepsilon = 0.02$ and $\omega_2 = 2.00$. Definitely the small viscosity helps to damp out later on the oscillation mode corresponding to the eigenfrequency, and the beat will disappear. This fact, however, is unimportant in the present context, since if the droplet does not disintegrate before the viscous effects come into play, it will definitely not disintegrate later on either. Therefore, the inviscid approximation valid until $t < 10$ allows us to find the most dangerous oscillations of the droplet and clarify whether it breaks up or not.

By increasing the modulation amplitude very slightly to $\varepsilon = 0.04$, which is still below the critical value 0.09 for ε given above for the static case, a resonance-like behaviour can be excited. It leads to permanently growing non-linear oscillations (Fig. 4), and the drop finally disintegrates in the range of validity of the inviscid approximation in a similar manner as in the case of a static sound field. Non-linear effects can be observed in the same way by applying a modulation frequency ω_2 which is (nearly) equal to the drop's eigenfrequency $\omega_2^{(\text{res})}$ or $\omega_2^{(\text{Ray})}$. The discussion at the beginning of Section 6 will show that in such cases non-linear resonant effects could easily overbear viscous damping, and the restriction of Eq. (23) can be eased.

In Fig. 5 we show which values of the maximum of the equatorial radius $b_{\max}$ over the oscillations of the drop correspond to different ε and ω_2, and when droplet break-up takes place. For one and the same modulation amplitude ε several windows can be found, where the drop breaks up or remains intact. One may speculate on the nature of the boundary in the diagram, separating "lethal" configurations for the drop from such that are survived. There are parameter configurations with $\varepsilon = 0.10$ and beyond that do not lead to drop break-up, if an ultrasound field is
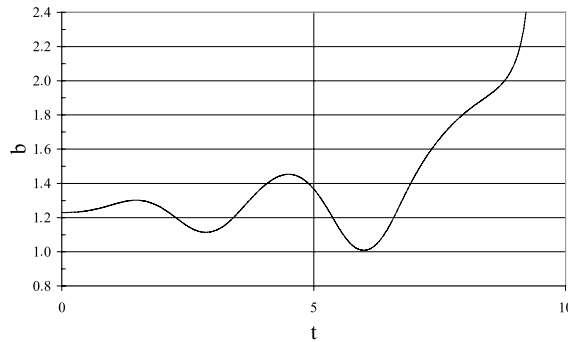
Fig. 4. The equatorial radius as a function of time for $\kappa = 0.575$, $B_a = 2.15$, $\varepsilon = 0.04$, and $\omega_2 = 2.0$.
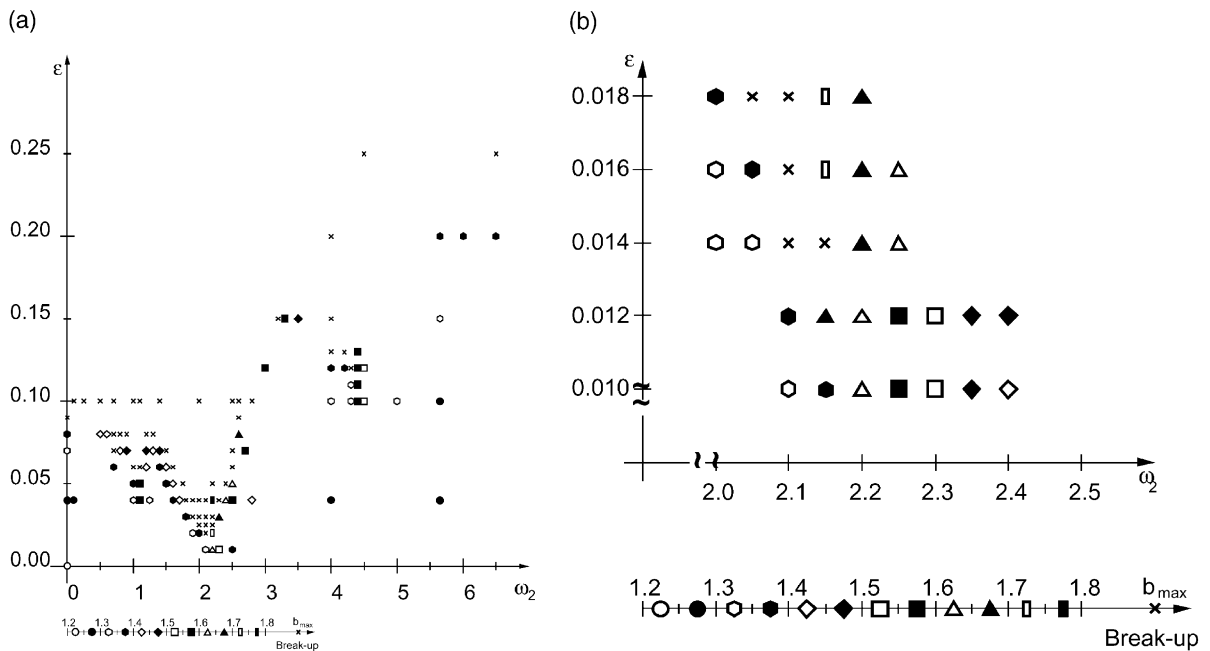

Fig. 5. Parameter configurations (ε, ω_2) that lead to drop break-up are marked by a cross; configurations that lead to drop oscillations are labelled by a symbol that indicates the maximum equatorial radius b_{max} during the oscillation. Fig. 5b is an enlarged detail from Fig. 5a; it can be concluded that the first drop eigenfrequency $\omega_2^{(res)}$ decreases with increasing modulation amplitude ε or oscillation amplitude.

modulated with an appropriate frequency ω_2. Bearing in mind that at $\omega_2 = 0$ no stable droplet configurations could be found with $\varepsilon > 0.09$, we can state that modulation of the acoustic field by $\omega_2 \neq 0$ may yield a dynamic stabilization of droplets preventing their break-up. In particular, if ω_2 is sufficiently high, the drop dynamics becomes very complicated and rich, but the drop does not necessarily disintegrate (at least within times considered during the simulations, which cover the range of validity of the inviscid approximation; viscous effects definitely cannot change this fact).

Drop break-up under the influence of ultrasound modulation occurs in most cases in a way which is analogous to the one sketched above for static ultrasound field, i.e. by squeezing the drop and pinching-off a torus-shaped liquid volume at the equator. Such a scenario is presented in Fig. 4.

Under particular conditions, another break-up scenario than described above can be observed. In this case the drop is squeezed to some extent, it then develops to a shape similar to a ring with a thin membrane in it. The membrane can break, causing a topological change of the drop volume. Our simulation then breaks down. After all, it is to be expected that in reality the break-up process of the membrane will break the cylindrical symmetry initially imposed to the problem. The break-up scenario described here is rather similar to one that has been observed experimentally, but for a static ultrasound field (Anilkumar et al., 1993). It should also be noted that Marston and Goosby (1985), in their experiments with liquid–liquid systems in modulated sound field, demonstrated still another break-up mode: via fissioning into two drops by pinching off at the equator. In their experiments equilibrium shapes tended to be prolate (instead of oblate in the present work), which might be the reason for the break-up mode.

It is emphasized that the eigenfrequency of the drop depends on the modulation amplitude ε or, equivalently, the oscillation amplitude. For $\varepsilon = 0.010$ we found $\omega_2^{(res)} \approx 2.20$, whereas for $\varepsilon = 0.012$ we obtained $\omega_2^{(res)} \approx 2.15$. This is another manifestation of the non-linear effects and in qualitative agreement with Trinh et al. (1996) as well as with Tsamopoulos and Brown (1983). It has the effect that the drop does not necessarily disintegrate even if the ultrasound field is modulated with a small (enough) amplitude and with the drop's eigenfrequency $\omega_2^{(res)}$, even though no dissipation and no damping is included at this time range. Moreover, the drop will not disintegrate when viscous effects manifest themselves.

The dynamics of the drop becomes apparently more complicated as the modulation amplitude is increased while ω_2 kept well away from the eigenfrequencies $\omega_l^{(res)}$. This can produce functions $b(t)$ where a non-trivial pattern is repeated several times virtually without modifications, see e.g. Fig. 6a (in the range of validity of the inviscid approximation), where a pattern of about $\Delta t = 8.57$ is repeated several times. These quasi-periodic cases are steps towards an even more complicated drop dynamics that occurs in particular at higher modulation frequencies; in the example is shown in Fig. 6b (also in the range of validity of the inviscid approximation), no periodicity at all can be recognized. Note also that the pattern in Fig. 6a seemingly corresponds to a case of subharmonic resonance between the driving frequency $\omega_2 = 1.5$ and its subharmonic $\omega_2/2 = 0.75$. As a result, periodicity with $\Delta t = 2\pi/0.75 \approx 8.37$ should arise, which is close to the value of $\Delta t = 8.57$ in Fig. 6a. A similar subharmonic resonance has been observed in the context of the forced oscillations of bubbles in Hall and Seminara (1980).

6. Oscillations of droplets levitated in monochromatically modulated acoustic field: comparison of calculated and measured shapes

In the experiment described in Section 2 the frequency of the amplitude modulation was taken the same as the eigenfrequency $\omega_2^{(Ray)}$. If a droplet were just a linear oscillator without viscous damping, it would show resonant oscillations of permanently growing amplitude at the excitation frequency leading to its break-up. In a sense, this could be a scenario similar to that of Fig. 4. In
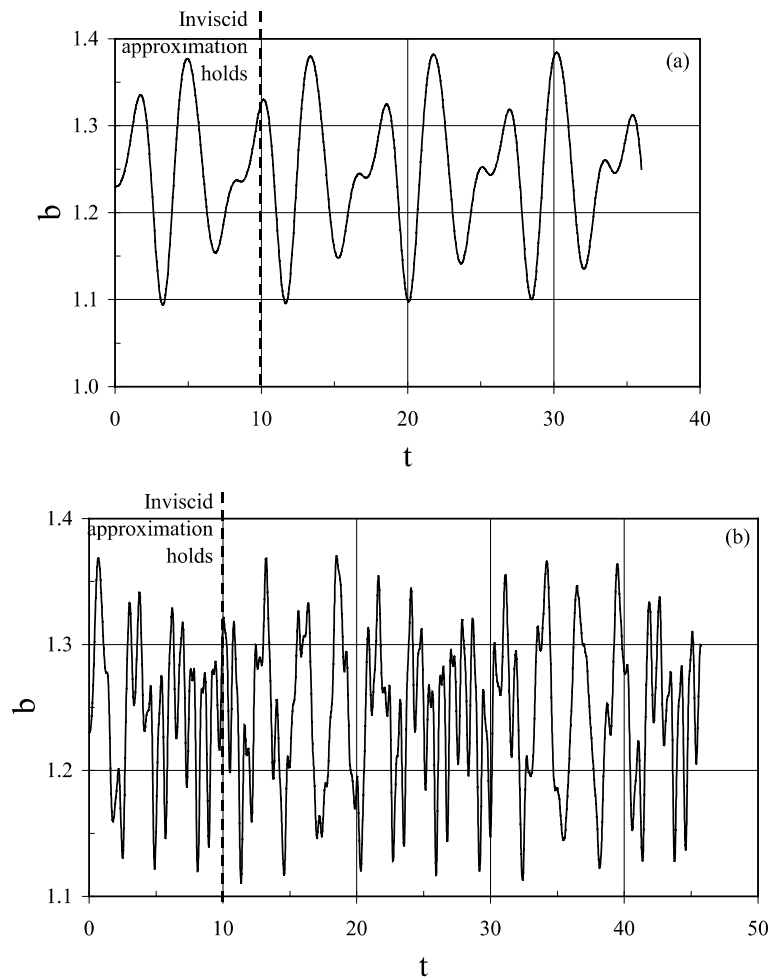
Fig. 6. (a) The equatorial radius as a function of time for $\kappa = 0.575$, $B_a = 2.15$, $\varepsilon = 0.05$, and $\omega_2 = 1.5$. A pattern of $\Delta t = 8.57$ is repeated several times virtually without modifications, a quasi-periodic case. (b) The equatorial radius as a function of time for $\kappa = 0.575$, $B_a = 2.15$, $\varepsilon = 0.20$, and $\omega_2 = 5.66$. No periodicity at all can be recognized any more.

this case all the other eigenmodes would just be overshadowed by the excited one. In reality, however, two effects counteract resonance break-up: (i) viscous damping, and (ii) the mechanism described in Section 5, when non-linearity at large amplitudes shifts the eigenfrequency and permanently detunes the droplet from resonance. Under appropriate conditions droplet break-up could then be prevented even at a resonant excitation. For low viscosity liquids that we are dealing with, viscous damping effects (i) can be expected to be negligible compared to the stabilization effects of non-linearity (ii). Therefore, the inviscid modeling of the present work should have a good chance to capture the excited drop oscillations during time intervals much larger than that estimated by Eq. (23). The present section is called for testing this opportunity.

First, a comparison of the length of the major and minor axes extracted from the images of the sequence depicted in Fig. 2 with theoretical values has been made. The measured lengths of both
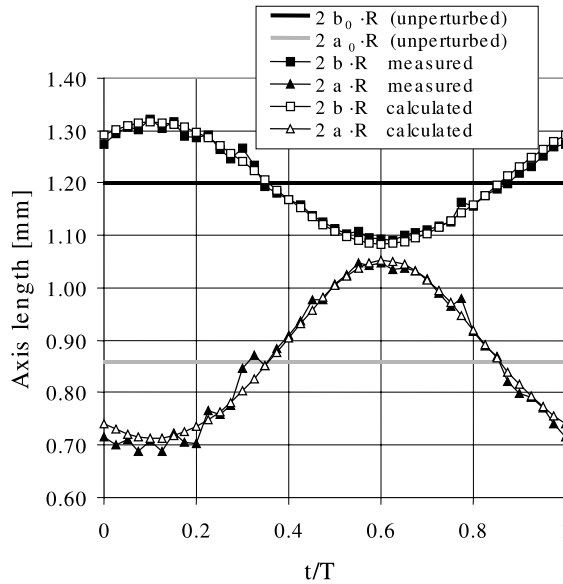
Fig. 7. Comparison between measured and calculated length of the dimensional major axis $2bR$ and minor axis $2aR$. The period of oscillation was about $T = 12.5$ ms, which is quite close to the value of 13 ms following from Eq. (1). The same drop as in Fig. 2; $\varepsilon = 0.005$, $\omega_2 = 5.0307$ (rendered dimensionless by $(g/R)^{**}$ (1/2)).

the major and minor axes and the corresponding theoretical values have been plotted in Fig. 7. The agreement is very good during the whole period of oscillation $T = 12.5$ ms, even though no viscous effects were accounted for in the modeling. This is a clear manifestation of the dominating role of the non-linear resonance-driving stabilization mechanism over the viscous effects.

As a next step, a comparison between calculated and measured droplet shapes has been made. The shapes are presented in the dimensionless coordinates defined in Section 3. Comparisons at 10 different dimensionless instants t/T in the oscillation period have been made and are depicted in Fig. 8. The agreement between the observed and the calculated shapes is seen to be excellent.

7. Sweeping case

We now modulate the ultrasonic field according to the law

$$A_0^{(\text{eff})} = A_0(1 + \varepsilon \sin \omega_2 t), \quad \text{again with} \, 0 < \varepsilon \ll 1, \tag{26a}$$

but with

$$\omega_2 = \omega_{20} + t \frac{d\omega_2}{dt}, \quad \text{where} \, \frac{d\omega_2}{dt} \, \text{is constant}, \tag{26b}$$

i.e. we sweep a window; with the modulation frequency ω_2 this window is chosen such that it contains the lowest eigenfrequency of the axisymmetric drop oscillations $\omega_2^{(\text{res})}$.
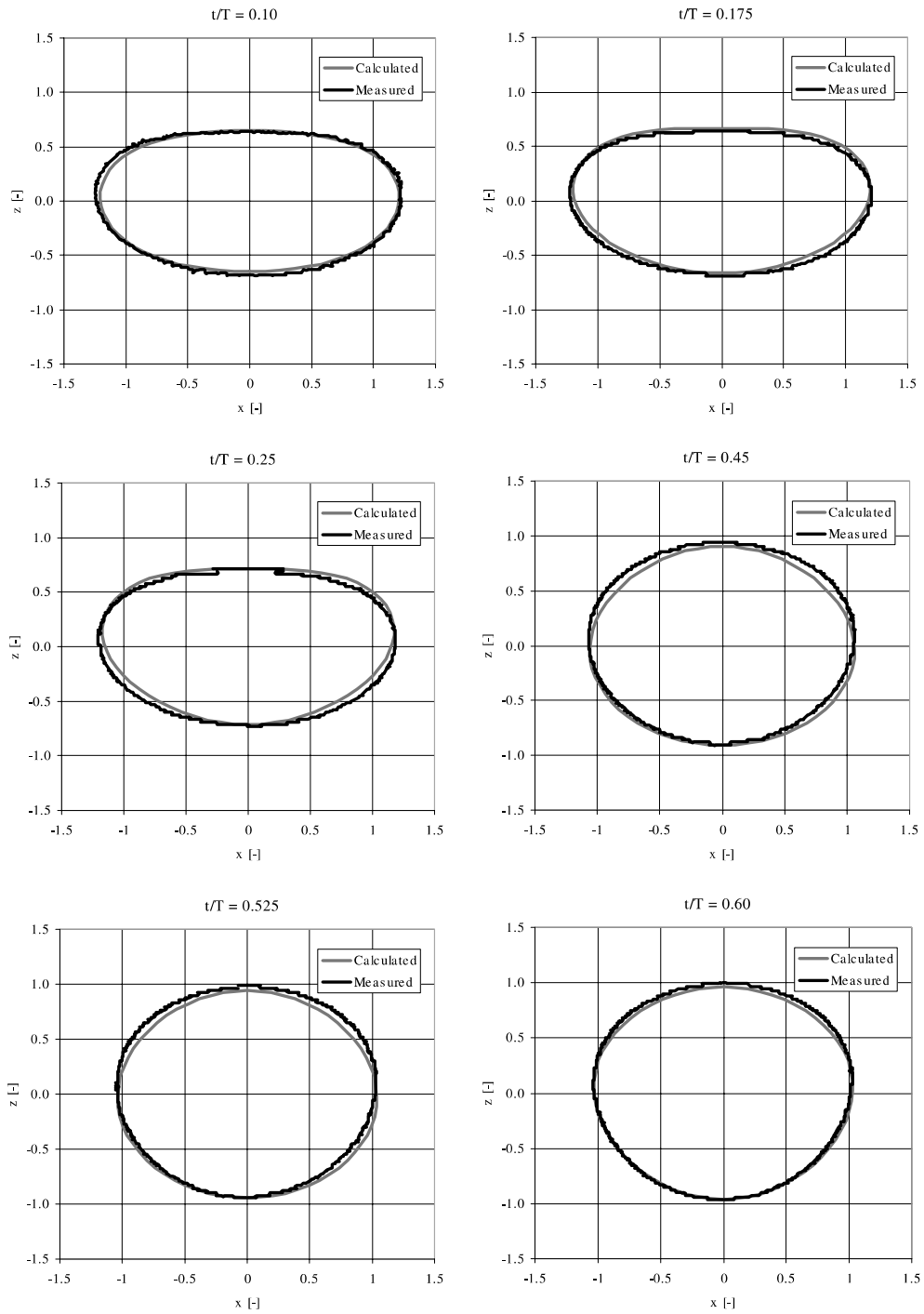
Fig. 8. Comparison between measured and calculated droplet shapes at different deformation stages. The dimensionless time t/T is given in each diagram. The coordinates x and z are rendered dimensionless by the radius of a volume equivalent sphere. The same drop as in Fig. 2; $\varepsilon = 0.005$, $\omega_2 = 5.0307$ (rendered dimensionless by $(g/R)^{**}$ (1/2)).
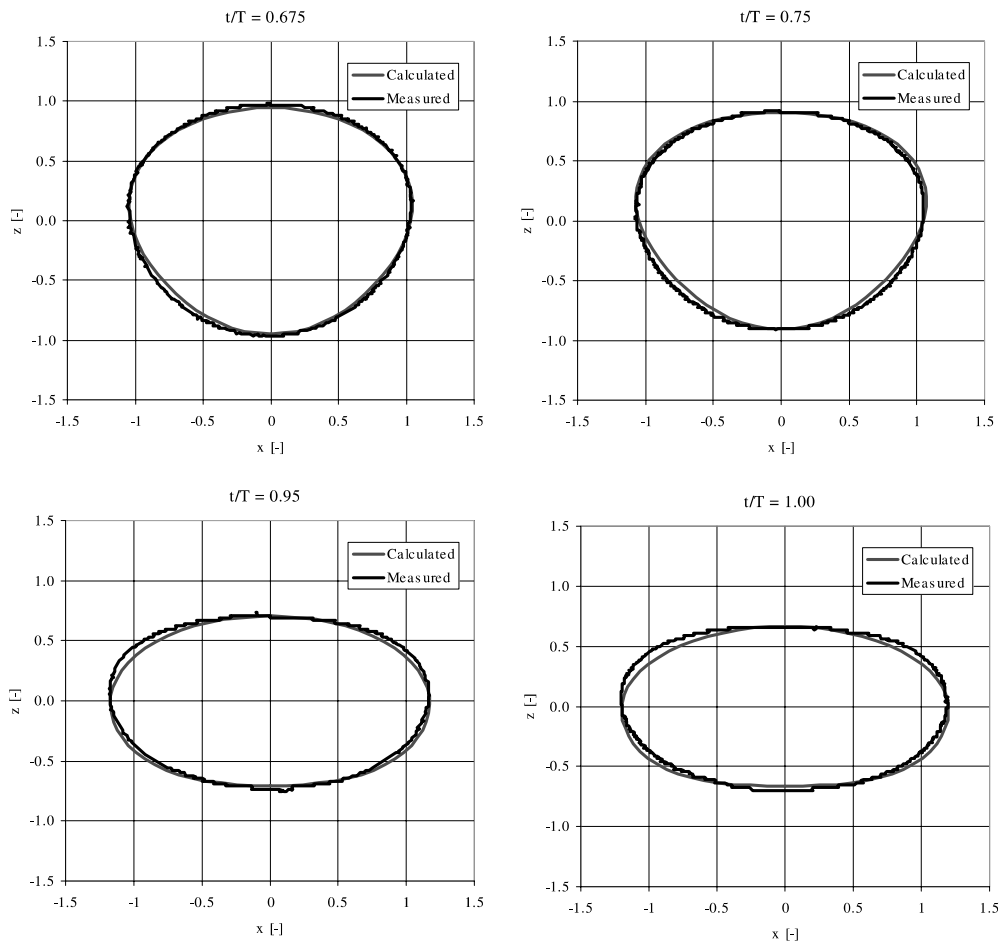
t/T = 0.675

t/T = 0.75

t/T = 0.95

t/T = 1.00

Fig. 8 (*continued*)

The simulations presented in this section are in the origin motivated by experiments performed in Daidzic et al. (1994). In spite of the fact that it is rather difficult to compare them directly to theoretical considerations (see the remarks in the Introduction), the parameters chosen there have been used for the simulations. In this way the wave number κ, the surface tension number S, etc. have been chosen according to the experimental parameters given in Daidzic et al. (1994). Sound pressure level A_0 as well as the modulation amplitude ε, however, had to be chosen by a guess, which are hoped to be as close as possible to the values used in the experiments and allowing e.g. for stable drop shape equilibria in the case when modulation was switched off. Furthermore, the sweeping rate $d\omega_2/dt$ had to be taken significantly (typically by a factor of 10 or 100) larger than in the experiments mentioned, in order to keep computation time handy. On the other hand, the sweeping rates used still lead to overall times (needed to sweep the whole range) that were far beyond the limit within which the inviscid approximation holds. One crucial task of these sim-

ulations, though, was to check whether the so-called jump-phenomenon, i.e. a sudden blow-up of the oscillation amplitude at some excitation frequency (different for up-sweep and down-sweep, Daidzic et al., 1994), could be reproduced or not; if it cannot be reproduced even without taking into account viscous effects, it cannot be expected to be reproduced with viscous effects included either.

We decided to take for the following simulations an acoustic Bond number of $B_a = 1$, modulation amplitudes $0 < \varepsilon \leqslant 0.02$, and (dimensionless) sweeping rates $d\omega_2/dt = \pm 6.307 \times 10^{-3}$ or $\pm 3.1535 \times 10^{-2}$. Given that $t \lesssim O(1)$ per cycle of the drop oscillation, the sweeping rates taken here can be considered to be slow and virtually quasistatic.

In Fig. 9 we plot the equatorial drop radius as a function of the modulation frequency for a down-sweep ($d\omega_2/dt < 0$) and an up-sweep ($d\omega_2/dt > 0$) for a moderate sweeping rate $d\omega_2/dt = \pm 6.307 \times 10^{-3}$ and a small modulation amplitude $\varepsilon = 0.002$. We consider, in particular, the envelope of the signal $b(\omega_2)$. It is evident that for both sweep directions the signal $b(t)$ tends towards an oscillation within fairly constant limits (still for the times when viscous damping is negligible). These limits are practically the same for the up-sweep and for the down-sweep. In particular we do not observe any signs of a "jump phenomenon" as described in Daidzic et al. (1994), i.e. a sudden blow-up of the envelope of $b(t)$ at a certain modulation frequency.

If the ultrasound pressure level is modulated with a constant frequency ω_2 of 5.036 or 5.980, we get the beats throughout the simulations, and the oscillations remain weak in the range of validity of the inviscid approximation (they will become even weaker when viscous effects come into play). This indicates that the energy transfer from the ultrasound to the drop oscillation is strongly restricted at these modulation frequencies, which are neatly distinct from $\omega_2^{(res)}$. Thus, in experiments with sweeping modulation frequency one is to expect an increase and subsequent decrease of the oscillation amplitude as a function of ω_2 when sweeping over the frequency $\omega_2^{(res)}$. In reality, after sweeping over $\omega_2^{(res)}$ energy, flux from the sound field to the oscillations will be detached, and viscous damping will suppress oscillations for the values of ω_2 distant from $\omega_2^{(res)}$.

The same scenario as in Fig. 9 is essentially true for a slightly larger modulation amplitude of $\varepsilon = 0.005$. The increase of ε by a factor 2.5 leads to a similar increase in the range in which b oscillates.

An important detail evident from Fig. 9 is the fact that the envelope of the signal $b(\omega_2)$ takes its maximum at different frequencies (the maximum for the up-sweep is at a smaller ω_2 than that for down-sweep, indicating a finite width of the resonance curve). This fact has to be taken into account when resonant frequencies of drops, distorted under the influence of ultrasound, are to be determined.

The peaks in the envelope of the frequency-sweep response seen in Fig. 9 remind those of an undamped harmonic oscillator (cf. for example Fig. 3.4 in Pippard (1985)). Therefore the response of the droplet in this case is basically almost linear.

Increasing ε still further to 0.01 leads to the scenario depicted in Fig. 10. The up-sweep still saturates. The down-sweep, however, behaves differently. Still, b tends to oscillate between well-defined limits; the range connected with these limits is much wider in this case, though. For a still higher modulation amplitude of $\varepsilon = 0.02$, in the up-sweep the equatorial radius b oscillates in a range, the size of which is still roughly proportional to ε. The down-sweep, however, behaves very similarly to the one shown in Fig. 10b. However, the oscillation amplitude does not saturate. It
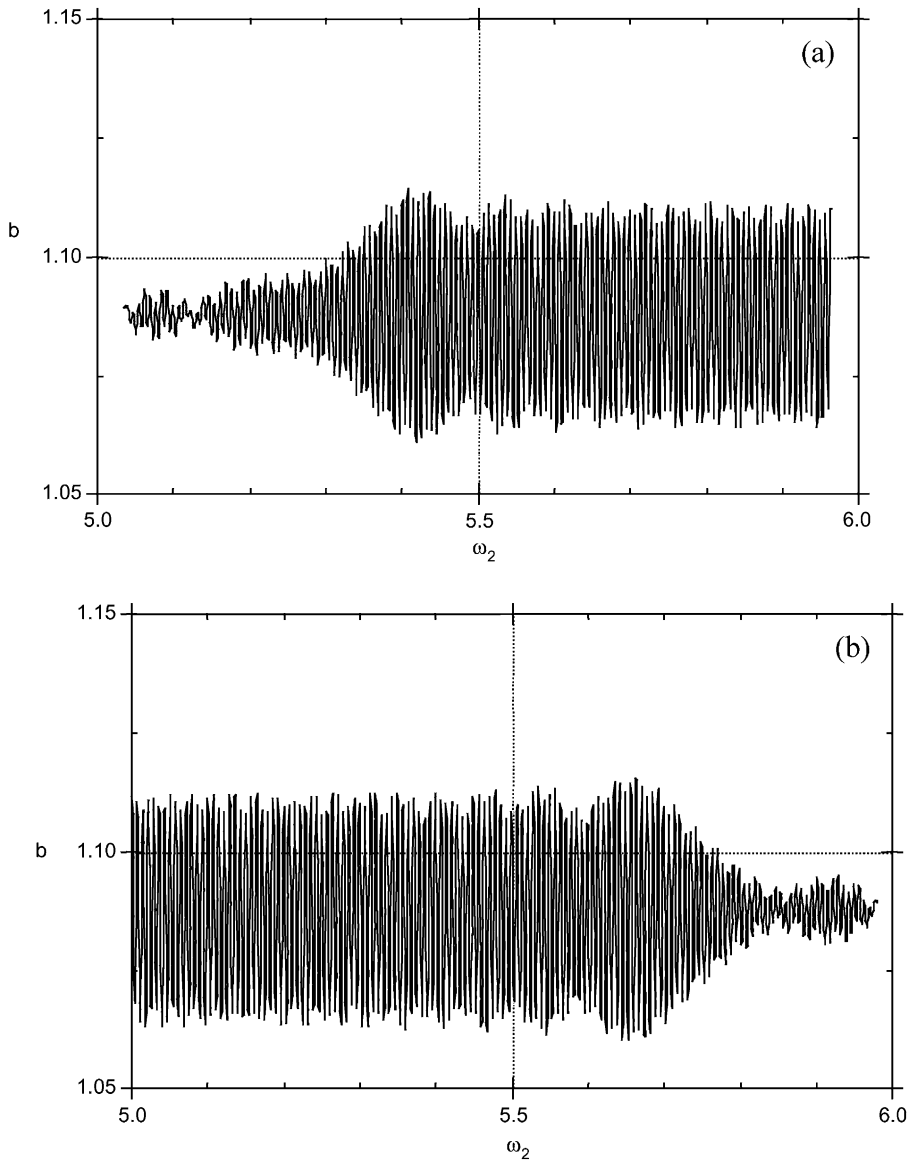
Fig. 9. Drop equatorial radius as a function of the instantaneous modulation frequency $\omega_2(t)$ on (a) up-sweep, i.e. $d\omega_2/dt > 0$, and b) down-sweep, i.e. $d\omega_2/dt < 0$. We take $S = 3.757$, $\kappa = 1.055$, $B_a = 1.00$; the modulation amplitude is $\varepsilon = 0.002$, the sweeping rate $d\omega_2/dt = \pm 6.307 \times 10^{-3}$ starting from $\omega_{20} = 5.036$ for the up-sweep and 5.980 for the down-sweep, respectively. In this case $\omega_2^{(res)} \approx 5.5$ (rendered dimensionless by $(g/R)^{**} (1/2)$).

blows up till the drop breaks up. It is emphasized that this break-up is not sudden, however, in the sense of the jump phenomenon described by Daidzic et al. (1994).

The dependence of the droplet behaviour on the sweeping rate is illustrated in Fig. 11. In spite of the fact that the modulation amplitude is the same as in Fig. 10, the range within which b oscillates after saturation is smaller and symmetric for up-sweep and down-sweep.
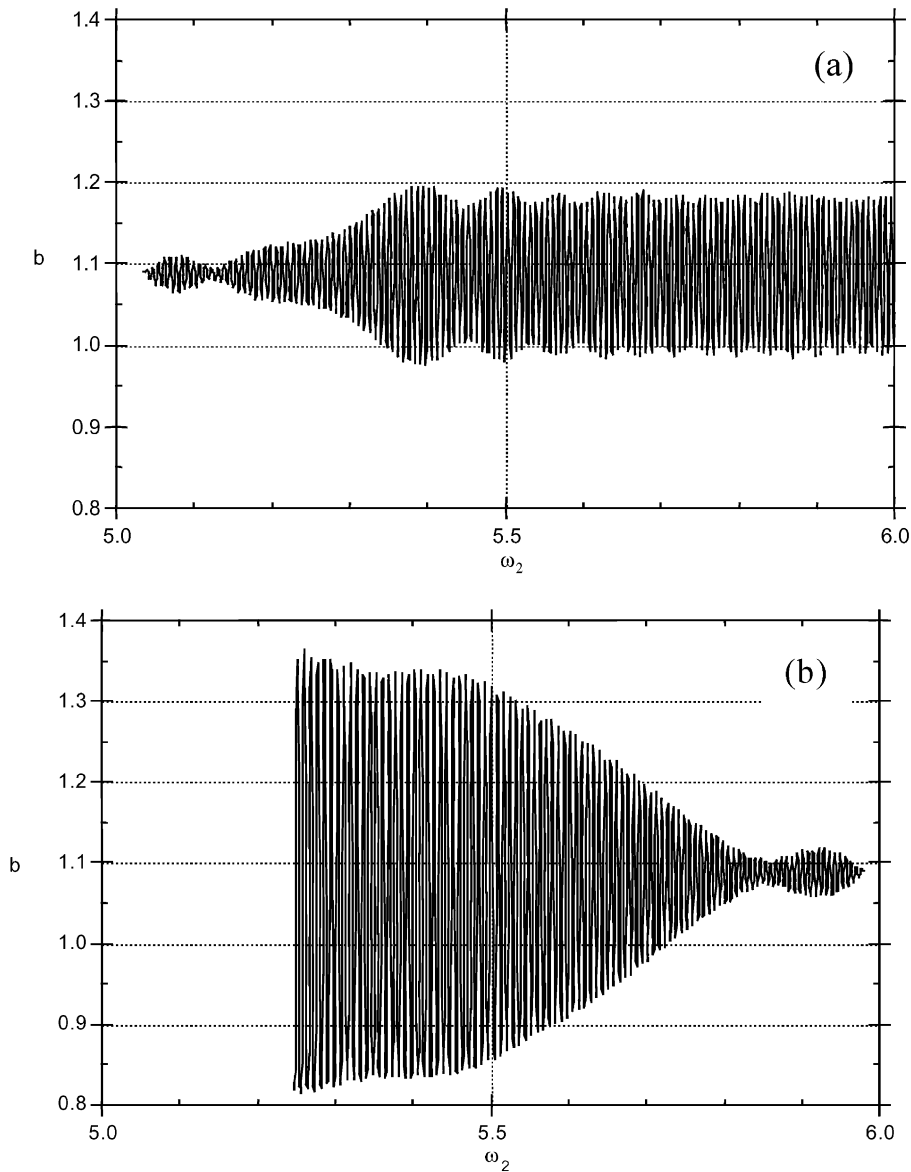
Fig. 10. Drop equatorial radius as a function of the instantaneous modulation frequency $\omega_2(t)$ on (a) up-sweep, i.e. $d\omega_2/dt > 0$, and (b) down-sweep, i.e. $d\omega_2/dt < 0$. Still we take $S = 3.757$, $\kappa = 1.055$, $B_a = 1.00$; the modulation amplitude is $\varepsilon = 0.01$ now, the sweeping rate $d\omega_2/dt = \pm 6.307 \times 10^{-3}$ starting from $\omega_{20} = 5.036$ for the up-sweep and 5.980 for the down-sweep, respectively. In this case $\omega_2^{(res)} \approx 5.5$ (rendered dimensionless by $(g/R)^{**}$ (1/2)).

These findings are summarized by stating that an asymmetric blow-up of the equatorial radius is observed if the sweeping-rate is sufficiently low and the modulation amplitude is sufficiently high.
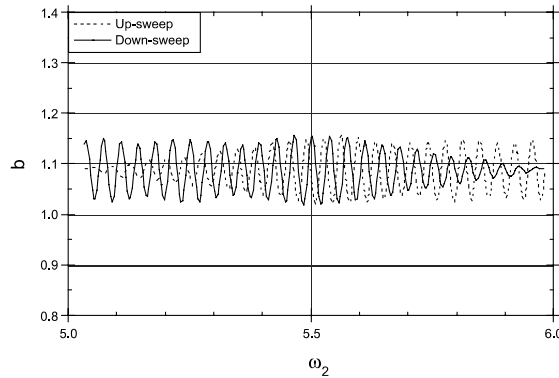
Fig. 11. Drop equatorial radius as a function of the instantaneous modulation frequency $\omega_2(t)$. Still we take $S = 3.757$, $\kappa = 1.055$, $B_a = 1.00$; the modulation amplitude is $\varepsilon = 0.01$, the sweeping rate $d\omega_2/dt = \pm 3.1535 \times 10^{-2}$ starting from $\omega_{20} = 5.036$ for the up-sweep and 5.980 for the down-sweep, respectively.

8. Conclusion

The effect of an ultrasound, modulated with a frequency which was comparable to the first few drop resonance frequencies, was considered. For relatively small modulation amplitudes, the results obtained agree very well with experimental findings. It has been demonstrated that droplets excited at the lowest eigenfrequency do not necessarily disintegrate. This non-linear phenomenon is related to the fact that at larger amplitudes the eigenfrequency changes, which leads to detuning from resonance conditions. Effects of viscous damping for low viscosity liquids are uncomparably weaker than the effect of non-linearity and can be neglected. For moderate modulation amplitude a very rich drop dynamics was observed. A resonant drop break-up before any viscous effects have come into play, could be triggered by an appropriate choice of the modulation frequency, although the effective acoustic Bond number remained below its critical value $B_a \approx 2.55$ for a static sound field. Crucial condition for the drop to break up was a sufficiently large modulation amplitude.

Finally the modulation frequency was changed linearly with time, sweeping over a window containing the drop's first eigenfrequency. In the range of the inviscid approximation the drop equatorial radius oscillated between well-defined saturation values. For small modulation amplitude ε the range of oscillation increased linearly with the modulation amplitude. For larger modulation amplitude, however, a substantial increase in the oscillation range of the drop equatorial radius to a new saturation range was observed in the case of down-sweep; the increase did not occur in up-sweeps of the modulation frequency for the modulation amplitudes used. This result again showed the crucial importance of the modulation amplitude ε, together with the sweeping rate $d\omega_2/dt$. The jump-phenomenon observed experimentally and described in literature could not be reproduced numerically here, as a minimum at the sweeping rates employed, which still differ significantly from those used in the experiments.

Acknowledgements

References

Anilkumar, A.V., Lee, C.P., Wang, T.G., 1993. Stability of an acoustically levitated and flattened drop: an experimental study. Phys. Fluids A 5, 2763–2774.

Becker, A.A., 1992. The Boundary Element Method in Engineering. A Complete Course. McGraw-Hill, London.

Becker, E., Hiller, W.J., Kowalewski, T.A., 1991. Experimental and theoretical investigation of large-amplitude oscillations of liquid droplets. J. Fluid Mech. 231, 189–210.

Chandrasekhar, S., 1961. Hydrodynamic and Hydromagnetic Stability. Clarendon, Oxford.

Daidzic, N., Stadler, R., Melling, A., Tropea, C., 1994. Non-linear droplet stability in atomization processes. Sixth International Conference on Liquid Atomization and Spray Systems, ICLASS-94, Rouen, France, pp. 142–149.

Feng, Z.C., Su, Y.H., 1997. Numerical simulations of the translational and shape oscillations of a liquid drop in an acoustic field. Phys. Fluids 9, 519–529.

Hall, P., Seminara, G., 1980. Non-linear oscillations of non-spherical cavitation bubbles in acoustic fields. J. Fluid Mech. 101, 423–444.

Lamb, H., 1932. Hydrodynamics. Cambridge University Press, Cambridge.

Landau, L.D., Lifshitz, E.M., 1987. Fluid Mechanics, second ed. Pergamon, Oxford.

Lee, C.P., Anilkumar, A.V., Wang, T.G., 1994. Static shape of an acoustically levitated drop with wave-drop interaction. Phys. Fluids 6, 3554–3556.

Lundgren, T.S., Mansour, N.N., 1988. Oscillations of drops in zero gravity with weak viscous effects. J. Fluid Mech. 194, 479–510.

Lyell, M.J., 1996. The hydrodynamic field due to forcing by modulated acoustic waves. Int. J. Multiphase Flow 22, 45–54.

Marr-Lyon, M.J., Thiessen, D.B., Marston, P.L., 1997. Stabilization of a cylindrical capillary bridge far beyond the Rayleigh–Plateau limit using acoustic radiation pressure and active feedback. J. Fluid Mech. 351, 345–357.

Marston, P.L., Apfel, R.E., 1979. Acoustically forced shape oscillation of hydrocarbon drops levitated in water. J. Colloid Interface Sci. 68, 280–286.

Marston, P.L., Apfel, R.E., 1980. Quadrupole resonance of drops driven by modulated acoustic radiation pressure—Experimental properties. J. Acoust. Soc. Am. 67, 27–37.

Marston, P.L., Goosby, S.G., 1985. Ultrasonically stimulated low-frequency oscillation and break-up of immiscible liquid drops: Photographs. Phys. Fluids 28, 1233–1242.

Murray, I.F., Heister, S.D., 1999. On a droplet's response to acoustic excitation. Int. J. Multiphase Flow 25, 531–550.

Pelekasis, N.A., Tsamopoulos, J.A., Manolis, G.D., 1991. Non-linear oscillations of liquid shells in zero gravity. J. Fluid Mech. 230, 541–582.

Pippard, A.B., 1985. Response and Stability. Cambridge University Press, Cambridge.

Rudnick, J., Barmatz, M., 1990. Oscillational instabilities in single-mode acoustic levitators. J. Acoust. Soc. Am. 87, 81–92.

Shi, T., Apfel, R.E., 1995. Oscillations of a deformed liquid drop in an acoustic field. Phys. Fluids 7, 1545–1552.

Shi, W.T., Apfel, R.E., 1996. Deformation and position of acoustically levitated liquid drops. J. Acoust. Soc. Am. 99, 1977–1984.

Shi, W.T., Apfel, R.E., Holt, R.G., 1995. Instability of a deformed liquid drop in an acoustic field. Phys. Fluids 7, 2601–2607.

Trinh, E.H., Holt, R.G., Thiessen, D.B., 1996. The dynamics of ultrasonically levitated drops in an electric field. Phys. Fluids 8, 43–61.

Trinh, E.H., Thiessen, D.B., Holt, R.G., 1998. Driven and freely decaying non-linear shape oscillations of drops and bubbles immersed in a liquid: experimental results. J. Fluid Mech. 364, 253–272.

Trinh, E., Wang, T.G., 1982. Large-amplitude free and driven drop-shape oscillations: experimental observations. J. Fluid Mech. 122, 315–338.

Trinh, E., Zwern, A., Wang, T.G., 1982. An experimental study of small-amplitude drop oscillations in immiscible liquid systems. J. Fluid Mech. 115, 453–474.

Tsamopoulos, J.A., Brown, R.A., 1983. Non-linear oscillations of inviscid drops and bubbles. J. Fluid Mech. 127, 519–537.

Weiss, D.A., Yarin, A.L., 1999. Single drop impact onto liquid films: Neck distortion, jetting, tiny bubble entrainment, and crown formation. J. Fluid Mech. 385, 229–254.

Yarin, A.L., 2001. Stationary d.c. streaming due to shape oscillations of a droplet and its effect on mass transfer in liquid–liquid systems. J. Fluid Mech. 444, 321–342.

Yarin, A.L., Brenn, G., Kastner, O., Rensink, D., Tropea, C., 1999. Evaporation of acoustically levitated droplets. J. Fluid Mech. 399, 151–204.

Yarin, A.L., Pfaffenlehner, M., Tropea, C., 1998. On the acoustic levitation of droplets. J. Fluid Mech. 356, 65–91.